

Linear stability analysis via simulated annealing and accelerated relaxation

M. Furukawa^{1, a)} and P. J. Morrison²

¹⁾*Faculty of Engineering, Tottori Univ., Minami 4-101, Koyama-cho, Tottori-shi, Tottori 680-8552, Japan*

²⁾*Department of Physics and Institute for Fusion Studies, Univ. Texas at Austin, TX, 78712, USA*

(Dated: 19 September 2022)

Simulated annealing (SA) is a kind of relaxation method for finding equilibria of Hamiltonian systems. A set of evolution equations is solved with SA, which is derived from the original Hamiltonian system so that the energy of the system changes monotonically while preserving Casimir invariants inherent to noncanonical Hamiltonian systems. The energy extremum reached by SA is an equilibrium. Since SA searches for an energy extremum, it can also be used for stability analysis when initiated from a state where a perturbation is added to an equilibrium. The procedure of the stability analysis is explained, and some examples are shown. Because the time evolution is computationally time consuming, efficient relaxation is necessary for SA to be practically useful. An acceleration method is developed by introducing time dependence in the symmetric kernel used in the double bracket, which is part of the SA formulation described here. An explicit formulation for low-beta reduced magnetohydrodynamics (MHD) in cylindrical geometry is presented. Since SA for low-beta reduced MHD has two advection fields that relax, it is important to balance the orders of magnitude of these advection fields.

Keywords: MHD, equilibrium, stability, simulated annealing, acceleration

^{a)}furukawa@tottori-u.ac.jp

I. INTRODUCTION

Simulated annealing (SA)¹ is a kind of relaxation method for obtaining equilibria, stationary states, of Hamiltonian systems. In noncanonical Hamiltonian systems such as non-dissipative fluid dynamics (see Ref. 2 for review), there exists Casimir invariants that foliate the infinite-dimensional phase space. The surface in the phase space on which each Casimir invariant takes a same value is called a Casimir leaf. A stationary state or an equilibrium of the system is given by an energy extremum on the Casimir leaf.^{3,4}

With SA, a set of artificial evolution equations is solved, which is derived from the original equations of the Hamiltonian system. The set of artificial evolution equations is constructed so that the energy of the system changes monotonically, while preserving the Casimir invariants. The idea of the artificial dynamics was proposed originally for obtaining stationary states of two-dimensional fluid flows⁵⁻⁷ and generalized in Ref. 1. In Ref. 1, the formulation of the artificial dynamics was considerably extended and made more workable by providing a means of including additional constraints and by introducing a smoothing kernel. There a variety of stationary states were obtained for two-dimensional vortex dynamics and associated two-layer problems. The terminology “simulated annealing” was introduced in this paper.

The noncanonical Hamiltonian structure of ideal magnetohydrodynamics (MHD) was first given in Ref. 8. For testing the idea of SA, the MHD Hamiltonian structure was first used^{9,10} for low-beta reduced MHD¹¹ in a two-dimensional rectangular domain with doubly periodic boundary conditions. Since low-beta reduced MHD has two fields, i.e., vorticity and magnetic flux function, the relaxation path to a stationary state becomes rather complex. However, the application was successful. Later it was extended to cylindrical geometry, and an equilibrium with magnetic islands was obtained.¹² Further, SA was applied to high-beta reduced MHD¹³ in toroidal geometry, and successfully used to obtain tokamak as well as toroidally averaged stellarator equilibria.¹⁴

The above results are based on the double bracket formulation of SA.¹⁵ However, another type of artificial dynamics method for calculating stationary states is metriplectic dynamics.^{15,16} This relaxation method was successfully applied to two-dimensional vortex dynamics and further to axisymmetric MHD equilibria¹⁷ described by the Grad-Shafranov equation.¹⁸⁻²⁰

From a more general point of view, minimization of a functional like the energy functional for SA in this paper, may be done by various methods such as a classical steepest-descent method and its extensions, the Nelder-Mead method²¹, genetic algorithms²² and many others developed in the context of machine learning. Although they can be used for minimizing the energy functional of the MHD systems, it may not be straightforward to preserve the Casimir invariants since these methods are not based on the Hamiltonian structure of the governing equations. Our method is a natural choice for the energy minimization on a Casimir leaf.

It is pointed out that because SA searches for an energy extremum, or an energy minimum in the MHD problems, it can be used not only for equilibrium calculations but also for stability analysis. Suppose an equilibrium is given by solving the Grad-Shafranov equation in toroidal geometry or, e.g., just as a trivial solution in cylindrical geometry. Then, suppose a perturbation is given to the equilibrium followed by the SA procedure. If the equilibrium is an energy minimum, SA will recover the original equilibrium. If not, SA will lead to another state that is an energy minimum, or at least will leave the original equilibrium in a sense of linear stability. Note that it is important to stay on the same Casimir leaf as the original equilibrium when giving the perturbation. Such perturbations were termed dynamically accessible in Refs. 23–25. If a perturbation is not dynamically accessible, SA will not recover the original equilibrium because the perturbed state is on another Casimir leaf. The SA procedure will find another equilibrium that is on the Casimir leaf where the perturbed state exists. In the present paper, the procedure for the stability analysis, especially how the perturbation is given without leaving the Casimir leaf, is developed.

On the basis of the previous studies, one would expect that SA can calculate a wide class of ideal MHD equilibria including magnetic islands and/or magnetic chaotic regions. Also, SA can be used for analysis of not only linear but also nonlinear stability. However, it is not so straightforward because SA solves an initial-value problem, and the numerical simulation of an initial-value problem generally takes time. Even in the linear stability analysis, it takes time to show that an equilibrium is stable since we have to observe that the given perturbation disappears. Therefore, an acceleration method is necessary for SA to be practically useful. In the present paper, an acceleration method is developed for the double bracket formulation of SA. The method is explicitly described for the low-beta reduced MHD model in cylindrical geometry, and applied to the stability analysis.

The paper is organized as follows. In Sec. II, the double bracket formulation of SA

for low-beta reduced MHD is introduced. Then the procedure for the stability analysis is explained in Sec. III. Section IV presents numerical results. Linear stability of a stable equilibrium is analyzed in Sec. IV A, while Sec. IV B is for an unstable equilibrium. An equilibrium, the stability of which is to be subsequently analyzed, is given in Sec. IV A 1, and a dynamically accessible perturbation is given to the equilibrium in Sec. IV A 2. Here it is explained how the dynamically accessible perturbation stays on the original Casimir leaf. Then, a preliminary result, one before an acceleration method is introduced, is presented, and the problem of slow convergence is explicitly shown in Sec. IV A 3. The slow convergence comes from an imbalance of relaxation speeds between the relaxing fields. In order to confirm this, simulation results where one field is eliminated is presented in Sec. IV A 4. Next, in Sec. IV A 5, the acceleration method is developed that balances the relaxation speeds, and numerical results are shown. Section IV A 6 shows numerical results with another initial condition where the kinetic energy perturbation is larger. As explained earlier, Sec. IV B shows that a given perturbation grows while the energy decreases by SA for an unstable equilibrium. Stability analyses via SA in this paper are examined in Section IV C. Section V concludes the paper.

II. MODEL

A. Low-beta reduced MHD and normalization

In this paper, the low-beta reduced MHD model¹¹ is investigated. We consider a cylindrical plasma with minor radius a and length $2\pi R_0$. The low-beta reduced MHD equations are

$$\frac{\partial U}{\partial t} = [U, \varphi] + [\psi, J] - \varepsilon \frac{\partial J}{\partial \zeta}, \quad (1)$$

$$\frac{\partial \psi}{\partial t} = [\psi, \varphi] - \varepsilon \frac{\partial \varphi}{\partial \zeta}, \quad (2)$$

where all physical quantities are normalized by using the length a , the magnetic field in the axial direction B_0 , the Alfvén velocity $v_A := B_0/\sqrt{\mu_0\rho_0}$ with μ_0 and ρ_0 being vacuum permeability and typical mass density, respectively, and the Alfvén time $\tau_A := a/v_A$. The cylindrical coordinates (r, θ, z) as well as the toroidal angle $\zeta := z/R_0$ are used. The inverse aspect ratio is defined as $\varepsilon := a/R_0$. The fluid velocity is $\mathbf{v} = \hat{\mathbf{z}} \times \nabla\varphi$, and the magnetic

field is $\mathbf{B} = \hat{\mathbf{z}} + \nabla\psi \times \hat{\mathbf{z}}$, where the unit vector in the z direction is denoted by $\hat{\mathbf{z}}$. The vorticity is $U := \Delta_{\perp}\varphi$ and the current density is $J := \Delta_{\perp}\psi$, where the Laplacian in the r - θ plane is denoted by Δ_{\perp} . The Poisson bracket for two functions f and g is defined as $[f, g] := \hat{\mathbf{z}} \cdot \nabla f \times \nabla g$.

The Hamiltonian structure for low-beta reduced MHD, which follows from that of Ref. 8, was first given in Refs. 26 and 27. The Hamiltonian is the summation of kinetic and magnetic energies as

$$H[\mathbf{u}] := \int_{\mathcal{D}} d^3x \frac{1}{2} \left\{ |\nabla_{\perp}(\Delta_{\perp}^{-1}U)|^2 + |\nabla\psi|^2 \right\}, \quad (3)$$

where \mathcal{D} is the domain of the cylindrical plasma. The Casimir invariants are

$$C_m := \int_{\mathcal{D}} d^3x \psi(\mathbf{x}, t), \quad (4)$$

$$C_v := \int_{\mathcal{D}} d^3x U(\mathbf{x}, t). \quad (5)$$

Furthermore,

$$C_1 := \int_{\mathcal{D}} d^3x f(\psi_h), \quad (6)$$

$$C_2 := \int_{\mathcal{D}} d^3x U g(\psi_h) \quad (7)$$

are also Casimir invariants when only single helicity components are included in the dynamics. Here f and g are arbitrary functions of a helical flux $\psi_h(\mathbf{x}, t) := \psi(\mathbf{x}, t) + \varepsilon r^2/(2q_s)$ for a specified safety factor of a rational number $q_s = m/n$ with m and n being a poloidal and a toroidal mode number, respectively.

B. Double bracket formulation of simulated annealing

We adopt simulated annealing, formulated by using a double bracket^{1,12,15}. For low-beta reduced MHD, the set of artificial evolution equations are conveniently given in the reduced following form:

$$\frac{\partial U}{\partial t} = [U, \tilde{\varphi}] + [\psi, \tilde{J}] - \varepsilon \frac{\partial \tilde{J}}{\partial \zeta}, \quad (8)$$

$$\frac{\partial \psi}{\partial t} = [\psi, \tilde{\varphi}] - \varepsilon \frac{\partial \tilde{\varphi}}{\partial \zeta}, \quad (9)$$

where the advection fields are defined as

$$\tilde{\varphi}(\mathbf{x}, t) := \int_{\mathcal{D}} d^3x' K_{1j}(\mathbf{x}, \mathbf{x}') f^j(\mathbf{x}', t), \quad (10)$$

$$\tilde{J}(\mathbf{x}, t) := \int_{\mathcal{D}} d^3x' K_{2j}(\mathbf{x}, \mathbf{x}') f^j(\mathbf{x}', t). \quad (11)$$

Here $j = 1$ or 2 , f^1 is the right-hand side of Eq. (1), f^2 is the right-hand side of Eq. (2), and (K_{ij}) is a kernel with a definite sign.

Note that the equations have the same form as those of the original low-beta reduced MHD; however, the advection fields are replaced by the artificial ones. The advection fields must be chosen so that the energy of the system changes monotonically, however, there are still a variety of choices through the kernel.

If (K_{ij}) is positive definite, the energy of the system decreases monotonically. On the other hand, Casimir invariants are preserved. In this study, we choose (K_{ij}) to be diagonal with its diagonal components given by

$$K_{ii}(\mathbf{x}, \mathbf{x}') = \alpha_{ii} g(\mathbf{x}, \mathbf{x}'), \quad (12)$$

for $i = 1$ and 2 , where $g(\mathbf{x}, \mathbf{x}')$ is a Green's function defined through

$$\Delta g(\mathbf{x}, \mathbf{x}') := -\delta^3(\mathbf{x} - \mathbf{x}'). \quad (13)$$

Here, Δ is the Laplacian and $\delta^3(\mathbf{x})$ is the Dirac's delta function in three dimensions, respectively.

III. STABILITY ANALYSIS PROCEDURE

In this section, the procedure for using SA to assess stability is explained. It consists of three steps.

The first step is to choose an equilibrium. Although SA has been used for obtaining equilibria; here the equilibrium can be given by any method. For example, any cylindrically symmetric state is a trivial equilibrium in a cylindrical plasma. Although unbeknownst beforehand, the chosen equilibrium can be either stable or unstable. Similarly, any solution to the Grad-Shafranov equation is a candidate equilibrium in axisymmetric toroidal plasma, one for which the SA stability method could be applied. Of course, we could also choose an equilibrium that is obtained by SA.

The second step is to perturb the equilibrium. The key point is to make the perturbation dynamically accessible, i.e., have it stay on the same Casimir leaf as the equilibrium whose stability is being analyzed. This is accomplished by time evolution of U and ψ under Eqs. (8) and (9) using arbitrary advection fields $\tilde{\varphi}$ and \tilde{J} that are different from Eqs. (10) and (11). This is possible because the Casimir invariants are preserved for any time evolution by the equations of the form (8) and (9) since they can be generated by the noncanonical Poisson bracket operator, the co-kernel of which projects onto the symplectic leaves. If we choose these advection fields in the form (10) and (11) with the kernel (K_{ij}) of a definite sign, then the energy changes monotonically and the Casimir invariants are preserved. For the arbitrary choices of $\tilde{\varphi}$ and \tilde{J} , the Casimir invariants are still preserved, although the energy need not change monotonically.

The final step is to perform SA. If the chosen equilibrium is an energy minimum state, which by Dirichlet's theorem is a stable equilibrium (cf. Ref. 2), SA starting from the perturbed state in the second step will recover the original minimum energy state. This is at least true when the perturbation is in a linear regime.

Note that SA can identify a linearly unstable case without a big computational cost since a given perturbation grows in time while the energy is decreased by SA. On the other hand, it is time consuming for a stable case since we have to observe that the given perturbation really disappears by SA. Even if the perturbation becomes smaller by the SA time evolution, the system cannot be said to be stable if the perturbation remains with a small amplitude.

Let us emphasize the importance of the perturbation being dynamically accessible, where the time evolution in the final step occurs on a Casimir leaf determined by the initial condition used for the SA procedure. If the perturbed state were on a different Casimir leaf, the time evolution of SA in the final step would not recover the original equilibrium.

IV. NUMERICAL RESULTS

A. A case of stable equilibrium

1. *A case study equilibrium for stability analysis*

In order to clearly explain the efficacy of our method, in the present paper we choose an equilibrium with cylindrical symmetry. Any cylindrically symmetric state is an equilibrium

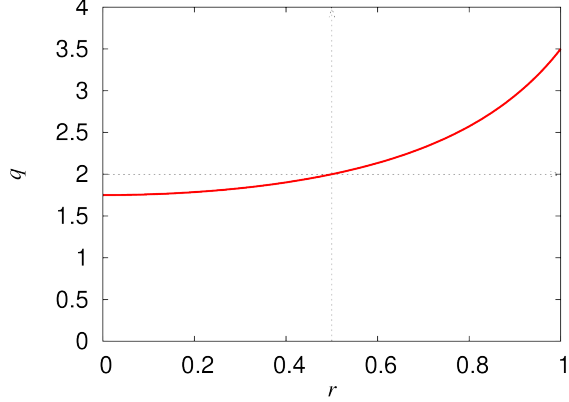


FIG. 1: Safety factor q profile.

of Eqs. (1) and (2). We assume that the equilibrium has no plasma rotation. The safety factor profile is assumed to be $q(r) = q_0/(1 - r^2/2)$ with $q_0 = 1.75$, and shown in Fig. 1. It has $q = 2$ surface at $r = 1/2$.

This equilibrium is spectrally stable against ideal MHD modes, although it is unstable to a resonant $(m, n) = (-2, 1)$ tearing mode. Note that we take the perturbed quantities proportional to $e^{i(m\theta+n\zeta)}$. Since SA does not change magnetic field line topology, we expect that SA will recover this equilibrium as an energy minimum state.

2. *Dynamically accessible perturbation of the equilibrium*

The equilibrium in the previous subsection IV A 1 is perturbed by using arbitrary advection fields, as explained in Sec. III. We choose the advection fields to be

$$\tilde{\varphi}(r, \theta, \zeta) = A_\varphi r(1 - r)e^{-\left(\frac{r-r_0}{L}\right)^2} \sin(2\theta - \zeta), \quad (14)$$

$$\tilde{J}(r, \theta, \zeta) = A_J r(1 - r)e^{-\left(\frac{r-r_0}{L}\right)^2} \cos(2\theta - \zeta), \quad (15)$$

where $A_\varphi = A_J = 10^{-3}$, $r_0 = 0.5$ and $L = 0.1$ are all fixed in time. The Fourier-decomposed radial profiles with this procedure are shown in Fig. 2.

The initial condition for the time evolution is the cylindrically symmetric equilibrium. Thus the $(m, n) = (-2, 1)$ components of U and ψ are generated in the beginning phase just after the time evolution is started. Then the nonlinear terms between the generated $(m, n) = (-2, 1)$ components and the $(m, n) = (-2, 1)$ modes of the advection fields generate the $(m, n) = (-4, 2)$ and $(0, 0)$ components. When the cylindrically symmetric equilibrium is perturbed in this way, the result stays on the same Casimir leaf.

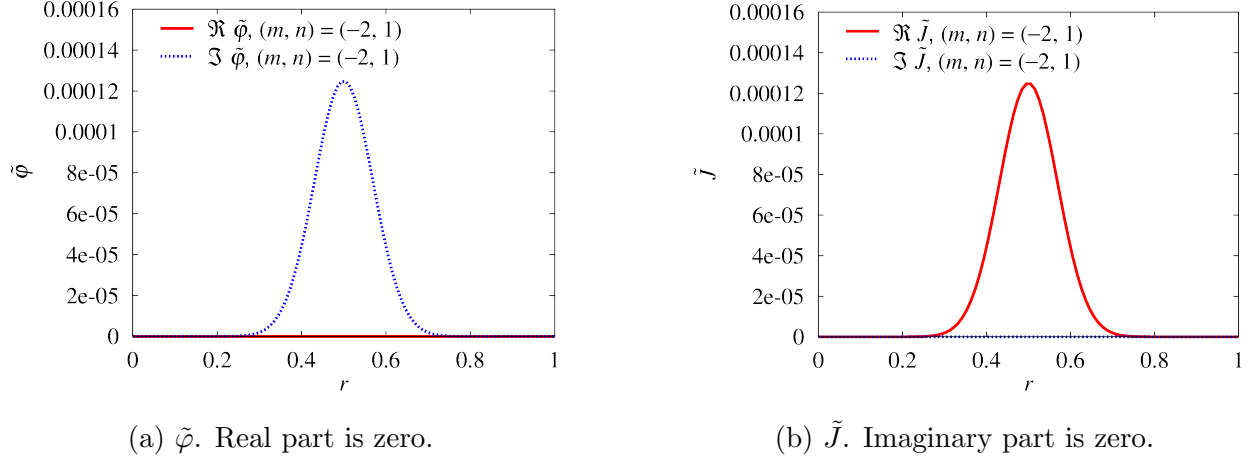


FIG. 2: Radial profiles of advection fields $\tilde{\varphi}$ and \tilde{J} used for generating dynamically accessible perturbations, i.e., perturbations on the same Casimir leaf as the equilibrium under consideration.

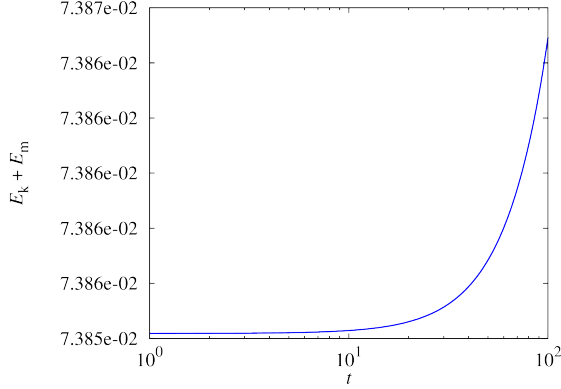
The time evolution of the total energy, the sum of the kinetic energy E_k and the magnetic energy E_m , and the magnetic helicity C_m , which is one of the Casimir invariants, are shown in Fig. 3. When the arbitrarily chosen advection fields in Eqs. (14) and (15) are used for perturbing the cylindrically symmetric equilibrium, we observe that the total energy increases in time, while the magnetic helicity remains constant.

In the remainder of Sec. IV, we perform SA to minimize the total energy of the system by using the advection fields Eqs. (10) and (11). The initial condition is chosen as the state at $t = 10$ in Fig. 3. The radial profiles are shown in Fig. 4.

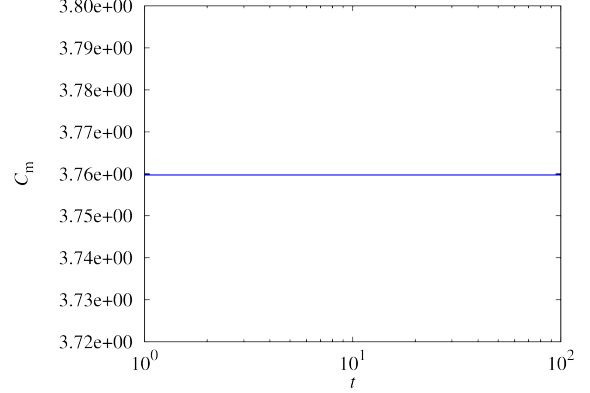
3. SA slow convergence of the velocity

Figure 5 shows the time evolution of total energy and the magnetic helicity during the SA evolution. Observe, the total energy monotonically decreases until the system appears to reach a steady state when the energy remains nearly constant for a long time. Note that the horizontal axis is a log scale. Therefore, the state seems to be an equilibrium that has the minimum energy. Also, Fig. 5 shows that the magnetic helicity does not change during the SA evolution.

Figure 6 shows the time evolution of radial profiles of the $(m, n) = (-2, 1)$ components of (a) $\Im U$, (b) $\Im \varphi$, (c) $\Re \psi$ and (d) $\Re J$, respectively. Note that $\Re U_{-2,1}$, $\Re \varphi_{-2,1}$, $\Im \psi_{-2,1}$ and



(a) The total energy increases in time, where E_k and E_m are kinetic and magnetic energies, respectively.



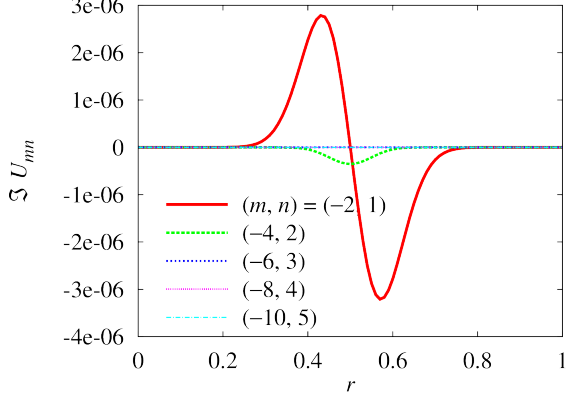
(b) Magnetic helicity C_m does not change in time.

FIG. 3: Time evolution of the total energy and the magnetic helicity, where the arbitrary chosen advection fields (14) and (15) are used for perturbing the cylindrically symmetric equilibrium.

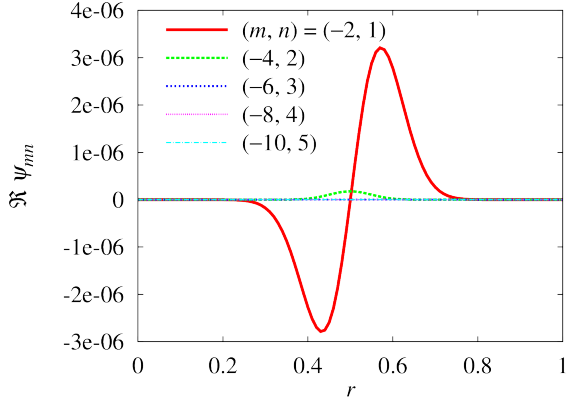
$\Im J_{-2,1}$ remain almost zero during SA. Even though the total energy starts to decrease just after the SA is started, the velocity components do not change visibly in the early stage. The change of the velocity components become visible even after the total energy reaches the stationary state, with these components changing even at $t = 5 \times 10^4$. On the other hand, the magnetic components start to decrease in the early stage of SA. Although $\Re J_{-2,1}$ still remains finite at $t = 3 \times 10^4$, the magnetic components are negligibly small at $t = 5 \times 10^4$. Thus, the rates of change of the velocity and magnetic components are significantly different.

This may be explained as follows. It is firstly pointed out that the $(m, n) = (-2, 1)$ components of U and ψ , the dominant Fourier modes of the perturbation, are $\mathcal{O}(10^{-6})$. Then φ is $\mathcal{O}(10^{-8})$, while J is $\mathcal{O}(10^{-3})$. This is because φ is obtained by integrating U especially in the radial direction, while J is obtained by differentiating ψ . Let us consider the very early stage of SA. The $(m, n) = (-2, 1)$ component of f^1 , or the right-hand sides of Eq. (1), is generated mainly by the $[\psi_{00}, J_{-2,1}]$ term. On the other hand, the $(m, n) = (-2, 1)$ component of f^2 , or the right-hand sides of Eq. (2), is generated by the $[\psi_{00}, \varphi_{-2,1}]$ term. Thus the $(m, n) = (-2, 1)$ component of f^1 is much larger than that of f^2 .

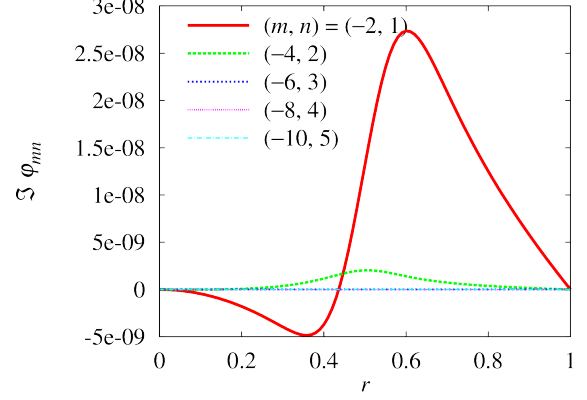
The artificial advection fields $\tilde{\varphi}$ and \tilde{J} are given by Eqs. (10) and (11), respectively. Since (K_{ij}) is taken to be diagonal in this study, the $(m, n) = (-2, 1)$ component of $\tilde{\varphi}$ is much



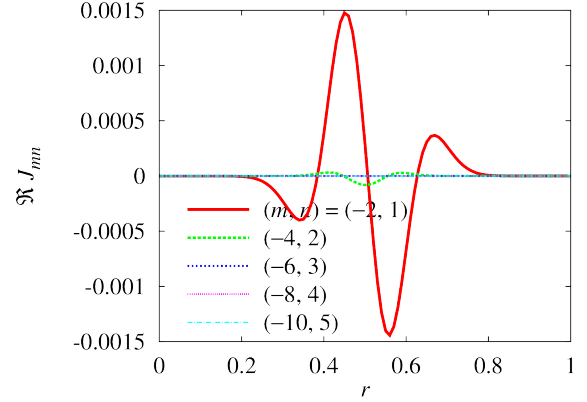
(a) Radial profile of $\Im U_{mn}$. The real part is zero.



(c) Radial profile of $\Re \psi_{mn}$. The imaginary part is zero.



(b) Radial profile of $\Im \varphi_{mn}$. The real part is zero.



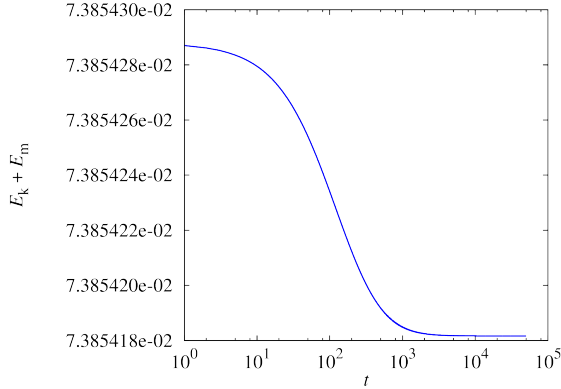
(d) Radial profile of $\Re J_{mn}$. The imaginary part is zero.

FIG. 4: Radial profiles of the perturbed state that is used as an initial condition for SA.

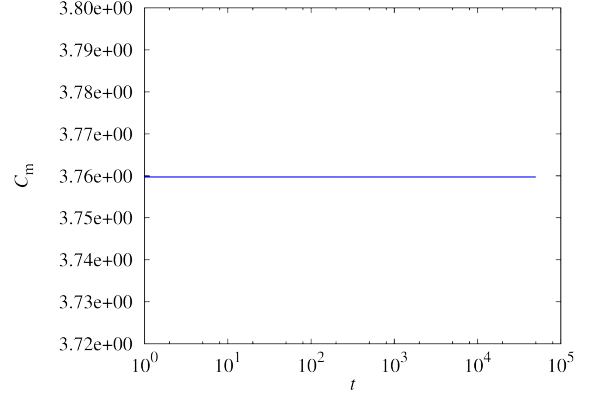
The $(m, n) = (-2, 1)$ components are dominant, but they still have small amplitudes.

larger than that of \tilde{J} . Then, in the SA equations (8) and (9), the $[\psi_{00}, \tilde{\varphi}_{-2,1}]$ term in Eq. (9) is much larger than the $[\psi_{00}, \tilde{J}_{-2,1}]$ term in Eq. (8). Therefore $\psi_{-2,1}$ starts to change much faster than $U_{-2,1}$. Note that the $[U, \tilde{\varphi}]$ term is negligible especially in the early stage of the SA since U_{00} is zero initially.

The SA equations for reduced MHD have two advection fields. Therefore, depending on the relative magnitudes, the relaxation path can change. In the present settings, the relaxation of the magnetic component is much faster than the velocity component. This may be understood schematically by supposing the energy level corresponds to the height of a mountain with topography. Then, the perturbed state corresponds to a point somewhere



(a) The total energy monotonically decreases in time.



(b) Magnetic helicity C_m does not change in time.

FIG. 5: Time evolution plots of the total energy and magnetic helicity during the SA evolution.

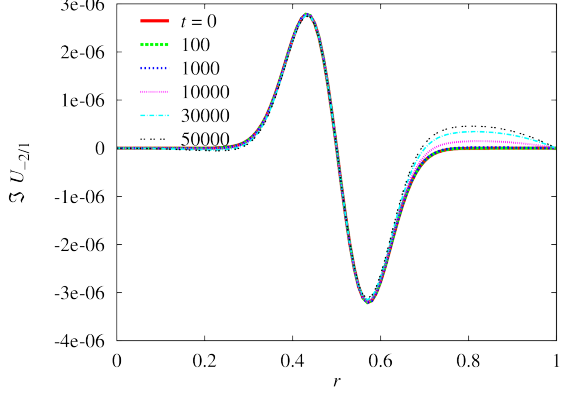
on a hillside of the mountain and the equilibrium is the place of the lowest height. There can be a variety of paths to the equilibrium. In the present case, the system goes down to the valley quickly, and then moves slowly along a valley to the place of the lowest height. Thus, the question is whether the path can be controlled without losing the characteristics of SA: monotonic change of the energy while preserving the Casimir invariants. This would be realized by forcing the two advection fields to have same order of magnitudes, which is what we will propose in Sec. IV A 5.

4. *SA relaxation with a forbidden direction*

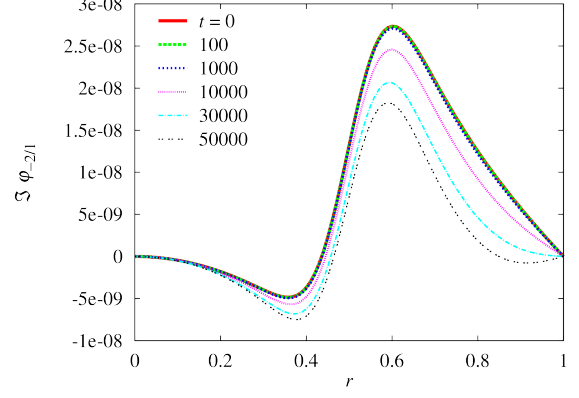
Before devising the advection fields that will speed up SA relaxation, let us first examine what happens if one of the advection fields is fully dropped. Since the system loses one of its fields for the relaxation, we expect the relaxation to be incomplete. Dropping one of the fields can be accomplished by setting either $\alpha_{11} = 0$ or $\alpha_{22} = 0$.

Figure 7 shows the time evolution of (a) total energy, (b) kinetic energy and (c) magnetic energy, respectively. The $\alpha_{11} = \alpha_{22} = 100$, the case of Fig. 5, is plotted here for comparison. Note that Fig. 7 is plotted onward from $t = 10^{-2}$ for showing clearly that initial energy is the same for all cases.

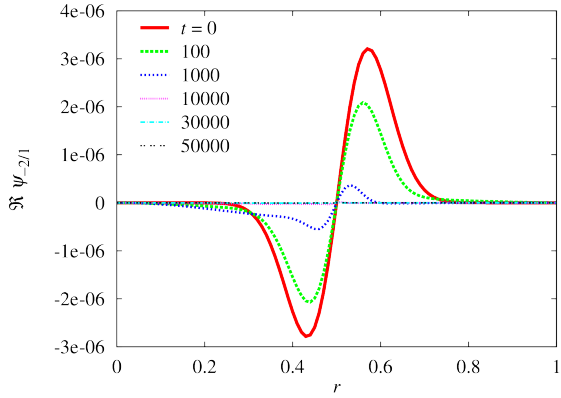
In the case of $\alpha_{11} = 0$ and $\alpha_{22} = 100$, $\tilde{\varphi}$ becomes zero. Then the magnetic energy does



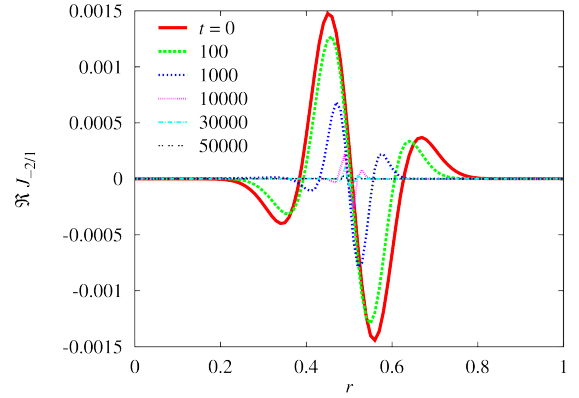
(a) Radial profile of $\Im U_{-2,1}$.



(b) Radial profile of $\Im \varphi_{-2,1}$.



(c) Radial profile of $\Re \psi_{-2,1}$. zero.

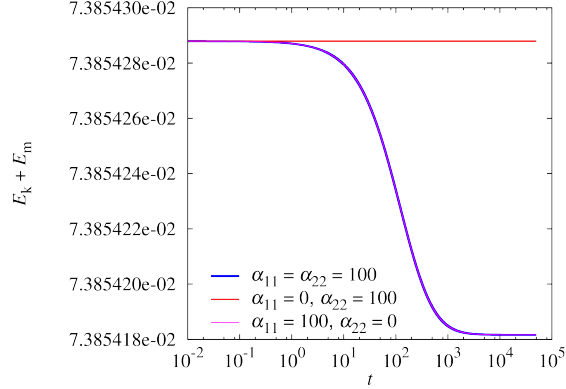


(d) Radial profile of $\Re J_{-2,1}$.

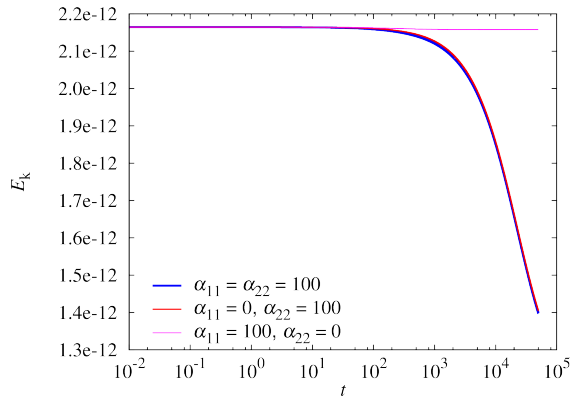
FIG. 6: Radial profiles of the $(m, n) = (-2, 1)$ components are plotted at several times during the SA evolution. The real parts of $U_{-2,1}$ and $\varphi_{-2,1}$ and the imaginary parts of $\psi_{-2,1}$ and $J_{-2,1}$ remain zero. The magnetic part $\Re \psi_{-2,1}$ and $\Re J_{-2,1}$ disappear relatively quickly, while the kinetic part $\Im U_{-2,1}$ and $\Im \varphi_{-2,1}$ are changing in the almost stationary state of the energy.

not change in time as shown in Fig. 7(c). This is clear from Eq. (9); ψ can only evolve with finite $\tilde{\varphi}$. Although the kinetic energy changes slightly due to the finite \tilde{J} as seen in Fig. 7(b), the total energy remains almost unchanged since the magnetic energy is dominant.

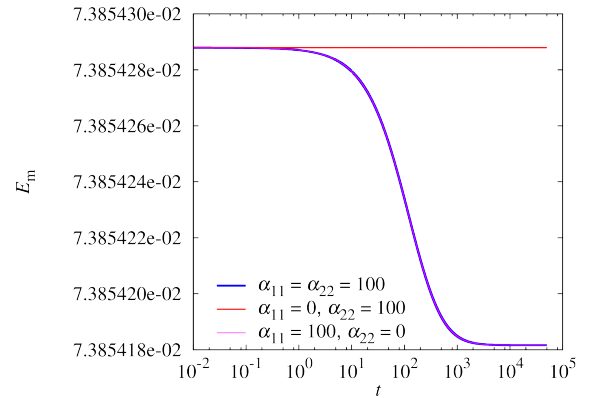
On the other hand, in the case of $\alpha_{11} = 100$ and $\alpha_{22} = 0$, \tilde{J} becomes zero. Then, the magnetic energy changes in time due to finite $\tilde{\varphi}$. The kinetic energy remains almost unchanged as seen in Fig. 7(b), although it can change slowly due to the nonlinear term $[U, \tilde{\varphi}]$ in Eq. (8). Since the relaxation of the dominant magnetic energy occurs in this case, the time evolution of the total energy almost overlaps the case of $\alpha_{11} = \alpha_{22} = 100$.



(a) Total energy.



(b) Kinetic energy.



(c) Magnetic energy.

FIG. 7: Time evolution of (a) total energy, (b) kinetic energy and (c) magnetic energy. If $\tilde{\varphi}$ is dropped by setting $\alpha_{11} = 0$, the dominant magnetic energy does not change and thus no relaxation occurs.

Summarizing, the magnetic energy can never decrease if $\tilde{\varphi}$ is completely dropped; thus the system does not relax to a minimum energy state. In the case of vanishing \tilde{J} , the system can relax, however, it must be quite slow. Therefore, both advection fields should remain finite and of comparable magnitude for obtaining efficient relaxation. This is the task addressed in Sec. IV A 5.

5. SA accelerated relaxation

Let us now consider a method for maintaining the advection fields to be of the same order of magnitude. In this study, we do this by introducing time dependence in the quantity (K_{ij})

of Eqs. (10) and (11), while retaining positive definiteness. Explicitly, we choose

$$\tilde{\varphi}(\mathbf{x}, t) := \alpha_{11}(t) \int_{\mathcal{D}} d^3x' g(\mathbf{x}, \mathbf{x}') f^1(\mathbf{x}', t), \quad (16)$$

$$\tilde{J}(\mathbf{x}, t) := \alpha_{22}(t) \int_{\mathcal{D}} d^3x' g(\mathbf{x}, \mathbf{x}') f^2(\mathbf{x}', t), \quad (17)$$

where $\alpha_{jj}(t)$ are chosen according to

$$\alpha_{jj}(t) = \min \left\{ \frac{F_{\max}}{\max_{r,m,n} |f_{mn}^j(r, t)|}, \alpha_{\max} \right\}. \quad (18)$$

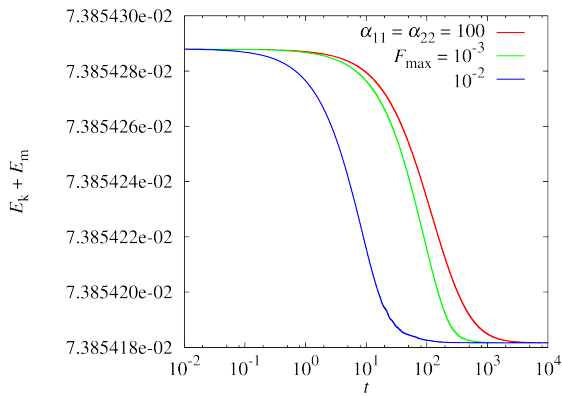
Here, $\max_{r,m,n} |f_{mn}^j(r, t)|$ is the maximum absolute value of the Fourier components of f^j in r and F_{\max} is the desired magnitude of the advection field. The parameter F_{\max} is taken to be the same for $j = 1$ and 2 for balancing the order of magnitude of $\tilde{\varphi}$ and \tilde{J} . Therefore, the first term in the curly braces controls the magnitude of the advection fields, forcing them to have the essentially the same order of magnitude. The second term in the curly braces is introduced to avoid divergence of the α_{jj} . In the final phase of the relaxation, $\max_{r,m,n} |f_{mn}^j(r, t)|$ becomes vanishingly small and the upper limit on α_{\max} avoids the divergence caused by this.

Figure 8 shows the time evolution of (a) total energy, (b) α_{11} and α_{22} , (c) kinetic energy and (d) magnetic energy for $F_{\max} = 10^{-3}$ and 10^{-2} . The time evolution of energy without the time dependence of α_{jj} , fixed $\alpha_{11} = \alpha_{22} = 100$, is also plotted in (a), (c) and (d). The upper limit for α_{jj} was set to $\alpha_{\max} = 10^7$. The convergence to the stationary state is clearly seen to be accelerated; for example, when $F_{\max} = 10^{-2}$, the required time for reaching the stationary state is considerably faster than the fixed α_{jj} case.

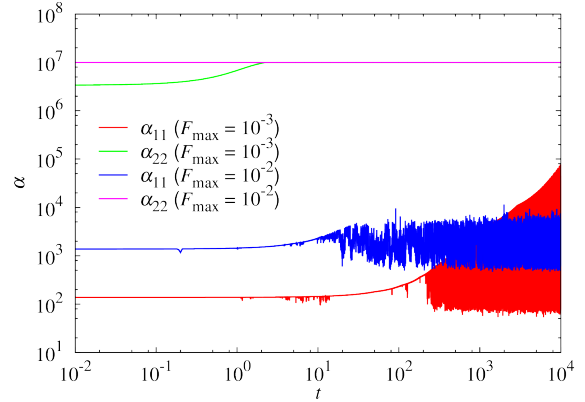
Especially, the time relaxation evolution of the kinetic energy starts significantly earlier than the $\alpha_{11} = \alpha_{22} = 100$ case as shown in Fig. 8(c), although the order of magnitude of the kinetic energy is small. In the case of fixed α_{jj} , the kinetic energy starts to decrease even after reaching the almost stationary state of the total energy. On the other hand, the kinetic energy starts to decrease in the early stage of SA when α_{jj} is varied in time.

As seen in Fig. 8(b), α_{22} is significantly larger than α_{11} . This is because f^2 is much smaller than f^1 . Accordingly, the rapid decrease of the kinetic energy is obtained.

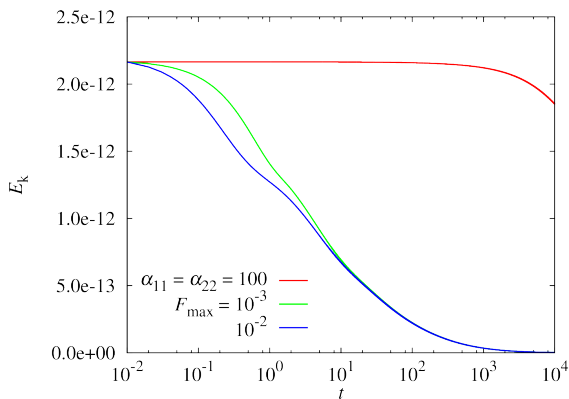
The choice of F_{\max} and α_{\max} can largely affect the convergence efficiency. If F_{\max} is too large, the simulation can diverge easily without an appropriate step-size control since the right-hand sides of the evolution equations (8) and (9) become too large. A large α_{\max} also



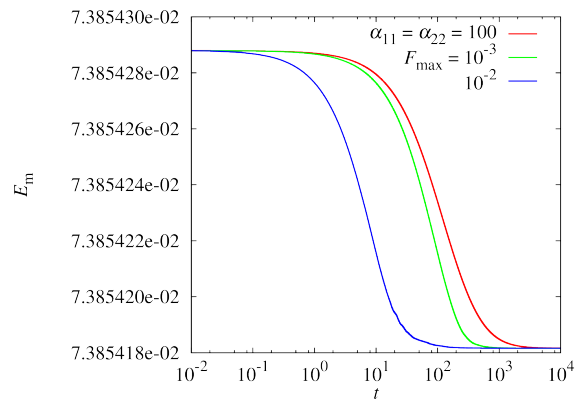
(a) Total energy.



(b) α_{11} and α_{22} .



(c) Kinetic energy.



(d) Magnetic energy.

FIG. 8: Time evolution of (a) total energy, (b) α_{11} and α_{22} , (c) kinetic energy and (d) magnetic energy for $F_{\max} = 10^{-3}$ or 10^{-2} . The upper limit was set to $\alpha_{\max} = 10^7$. The convergence to the stationary state is accelerated.

has similar tendency, although the effect on the divergence is indirect since α_{\max} is an upper limit for the right-hand sides of the evolution equation (8) and (9).

Related to the convergence efficiency, there can be a better choice for α_{jj} than that of Eq. (18). For example, one can expect defining α_{jj} for each m and n as $\alpha_{jj,mn}$. However, this is not so straightforward since $\max_r |f_{mn}^j(r, t)|$ becomes smaller for larger m and n and thus $\alpha_{jj,mn}$ can become huge or reach the upper limit. This means that the relative magnitude of the right-hand side associated with the evolved quantity U_{mn} or ψ_{mn} becomes large. Then the simulation is likely to diverge. In this case, F_{\max} and α_{\max} should be also chosen to have an appropriate order of magnitude for each U_{mn} and ψ_{mn} .

Another possible choice for accelerating convergence is to take the symmetric kernel (K_{ij})

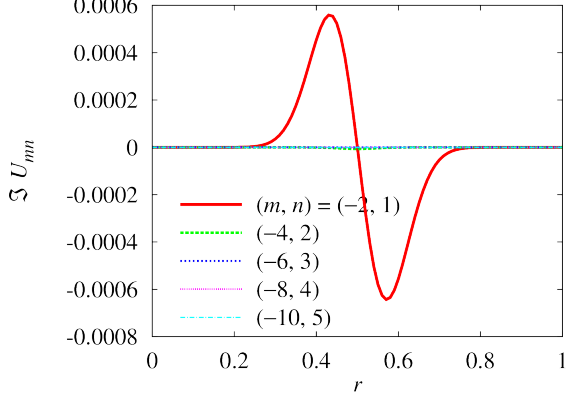
in Eqs. (10) and (11) with nonzero off-diagonal elements. This mixes f^1 and f^2 and can make the advection fields $\tilde{\varphi}$ and \tilde{J} for SA to be of comparable magnitudes. We have not tried this choice yet. Time dependence of the kernel may be necessary even with this choice to accelerate the convergence near the energy minimum state.

6. SA with another initial perturbation with larger kinetic energy

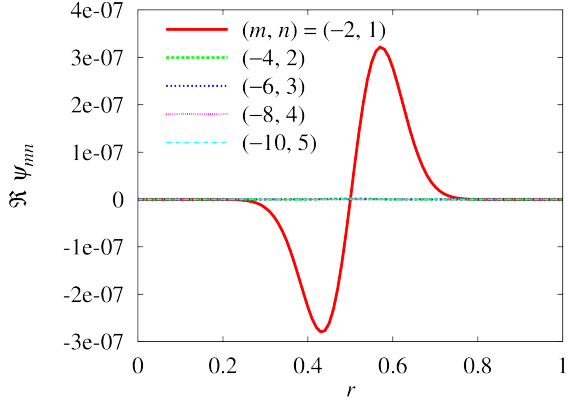
The SA results shown in the previous subsection IV A 5 were performed for the initial perturbation that has a larger perturbed magnetic energy ($\mathcal{O}(10^{-7})$) than the perturbed kinetic energy ($\mathcal{O}(10^{-12})$). In order to examine another case where the perturbed kinetic energy is larger than the perturbed magnetic energy, we chose a smaller $\tilde{\varphi}$ in Eq. (14) and a larger \tilde{J} in Eq. (15) for dynamically accessible perturbations. The total energy of the system increased by the advection. The radial profiles of the initial condition for SA are plotted in Fig. 9. The velocity part has about 200 times larger amplitudes and the magnetic part has about 10 times smaller amplitudes compared with Fig. 4. The perturbed kinetic energy is $\mathcal{O}(10^{-7})$, which is larger than the perturbed magnetic energy of $\mathcal{O}(10^{-9})$. They are still in a linear regime.

Starting from the initial state shown in Fig. 9, SA was performed. For the acceleration, $F_{\max} = 10^{-3}$ and $\alpha_{\max} = 10^7$ were used. The total energy decreased by SA as shown in Fig. 10. The simulation was stopped since the Fourier modes of the right-hand sides of Eqs. (8) and (9) for SA as well as the original low-beta reduced MHD Eqs. (1) and (2) became smaller than a threshold 10^{-8} , although the energy looks still to be decreasing. Note that the horizontal axis is a log scale, thus the decrease of energy is not so rapid.

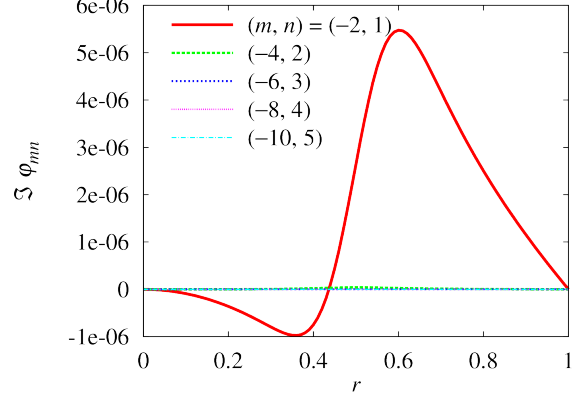
The perturbation amplitudes decreased in time as shown in Fig. 11. Since the initial magnetic perturbation was small in this case, the amplitudes of the magnetic part quickly became negligibly small. The velocity part is still changing, decreasing the kinetic energy, although it is already small. In fact, not shown in the presented figures, the magnetic energy became almost the same value as the cylindrically symmetric state, while the kinetic energy of $\mathcal{O}(10^{-9})$ still remained when the simulation was stopped. However, we observe that the amplitudes of the velocity part were disappearing. The decrease of total energy with the disappearance of perturbation again indicate that the equilibrium is stable.



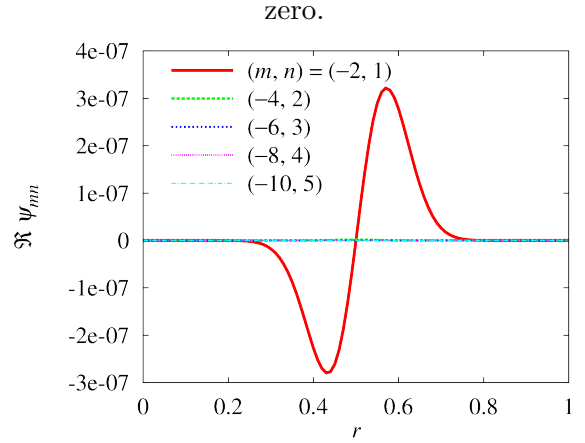
(a) Radial profile of $\Im U_{mn}$. The real part is zero.



(c) Radial profile of $\Re \psi_{mn}$. The imaginary part is zero.



(b) Radial profile of $\Im \varphi_{mn}$. The real part is zero.



(d) Radial profile of $\Re J_{mn}$. The imaginary part is zero.

FIG. 9: Radial profiles of the perturbed state that is used as an initial condition for SA. The $(m, n) = (-2, 1)$ components are dominant, but they still have small amplitudes.

B. A case of unstable equilibrium

In this subsection, SA is performed for linear stability analysis of an unstable equilibrium. The safety factor profile is the same as Fig. 1. The poloidal rotation profile is given by

$$v_{\theta}(r) = \frac{v_{\theta\max}(\alpha + 1)^{\alpha+1}}{\alpha^{\alpha}} r(1 - r)^{\alpha}, \quad (19)$$

where α is a positive parameter. For the following numerical results, $v_{\theta\max} = 0.01$ and $\alpha = 3$ were used. The profile is plotted in Fig. 12.

This equilibrium was perturbed by the same advection fields of Eqs. (14) and (15) with the amplitudes shown in Fig. 2. The total energy of the system decreased by the dynamically

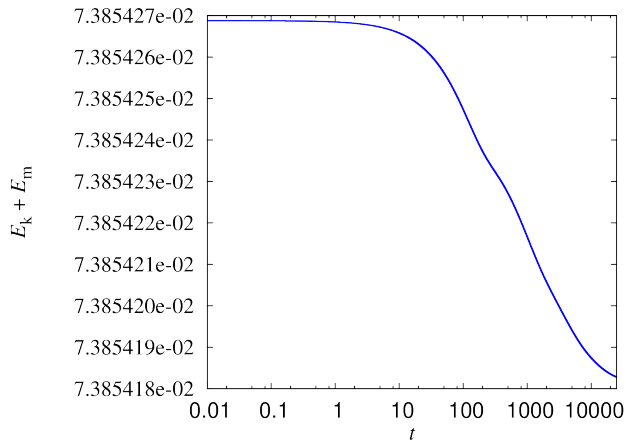


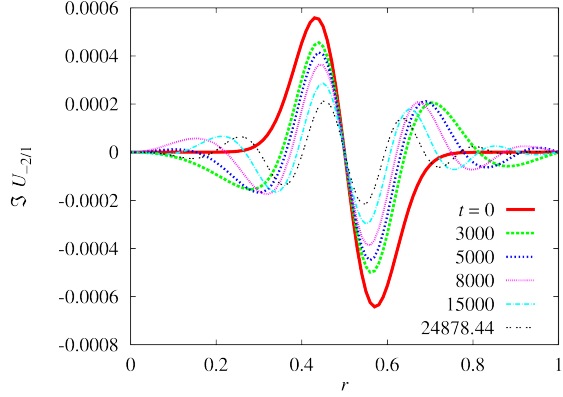
FIG. 10: The total energy decreased in time by SA. The perturbation amplitudes become smaller in time as shown in Fig. 11

accessible perturbation as shown in Fig. 13. This already means that there exists a state with a lower energy than the cylindrically symmetric equilibrium.

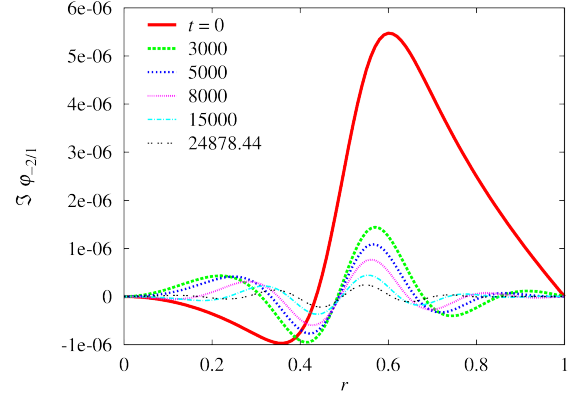
From a perturbed state with $t = 10$ in Fig. 13, we performed SA. The radial profiles of the initial condition for SA is shown in Fig. 14. The $(m, n) = (-2, 1)$ components are dominant, although the $(m, n) = (-4, 2)$ and $(m, n) = (-6, 3)$ components are still visible. The amplitudes are small and in a linear regime.

The time evolution of the total energy by SA is plotted in Fig. 15. The total energy decreased by SA. For the kernel of the double bracket, $F_{\max} = 10^{-3}$ and $\alpha_{\max} = 10^7$ were used. After $t \simeq 100$, the radial profiles of perturbed quantities started to oscillate in r , and the conservation of magnetic helicity was apparently violated. Therefore the time evolution is plotted only for $t \leq 100$. Linear eigenmode analysis without dissipation for this equilibrium gave us multiple unstable modes, although the numerical technique used was very simple. The eigenmodes look singular. The physical situation seems to be numerically difficult, and oscillation in r occurred.

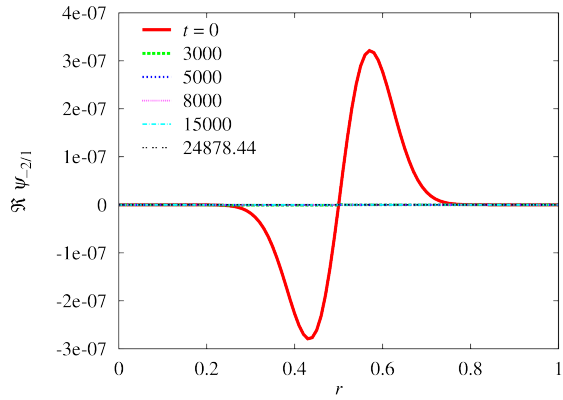
Although the total energy decreased in time by SA, the perturbation amplitudes grew in time as shown in Fig. 16. As noted above, the radial profiles started to oscillate after $t \simeq 100$, and thus another equilibrium without cylindrical symmetry was not obtained. However, the growth of the perturbation under decreasing energy shows that the original equilibrium is at least linearly unstable.



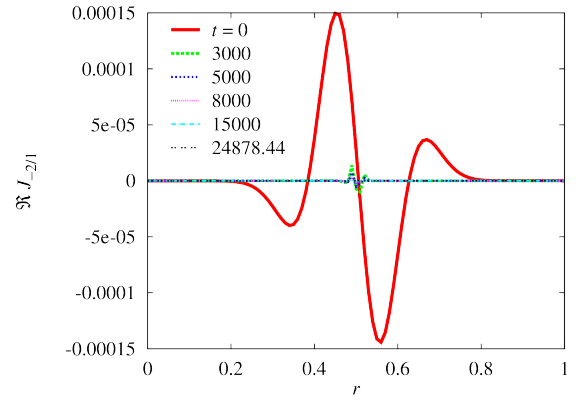
(a) Radial profile of $\Im U_{-2,1}$.



(b) Radial profile of $\Im \varphi_{-2,1}$.



(c) Radial profile of $\Re \psi_{-2,1}$.



(d) Radial profile of $\Re J_{-2,1}$.

FIG. 11: Radial profiles of the $(m, n) = (-2, 1)$ components are plotted at several times during SA evolution. The perturbation amplitudes decreased in time.

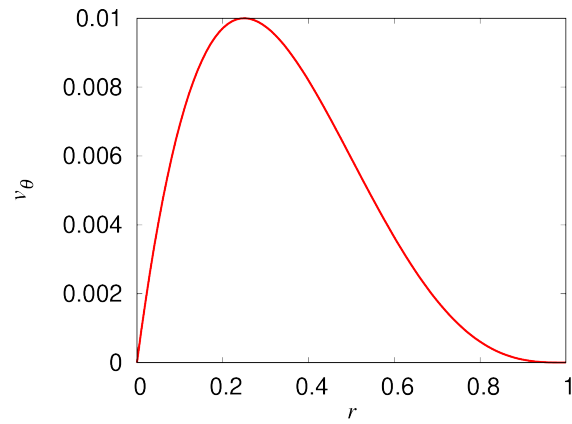


FIG. 12: Poloidal rotation velocity v_θ profile.

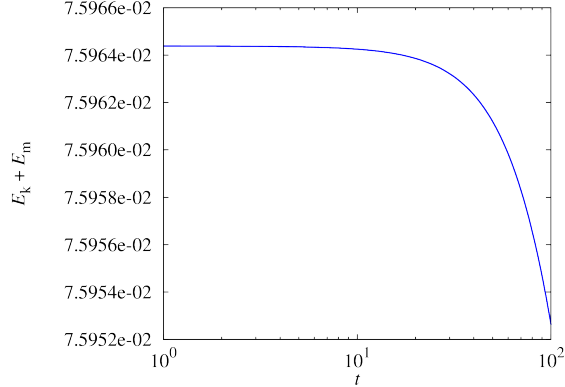


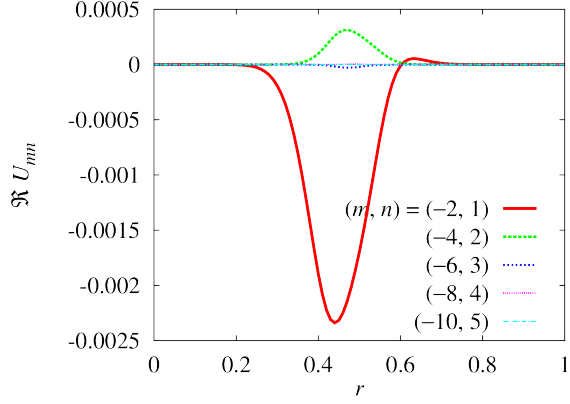
FIG. 13: The total energy decreased in time by the dynamically accessible perturbation.

C. Stability of equilibrium via SA

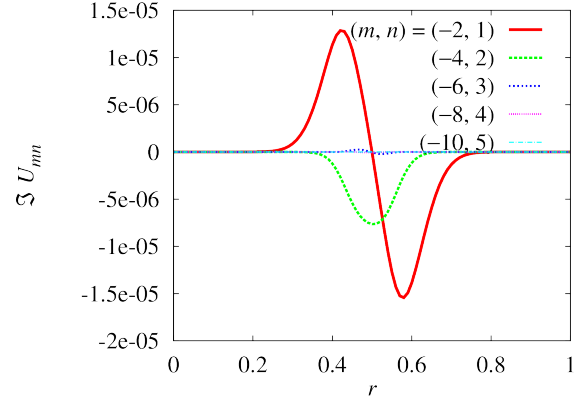
Let us now consider how SA can be used to find a stable equilibrium. Finding a stable equilibrium is rather time consuming since we have to observe that the given perturbation actually disappears by SA. We tried two kinds of dynamically accessible perturbations: one with a larger perturbed magnetic energy, the other with a larger perturbed kinetic energy, although both are still in a linear regime. In particular, we consider the equilibrium state obtained in Sec. IV A 5, which has almost zero kinetic energy, it being $\mathcal{O}(10^{-15})$. Also the magnetic energy reaches the stationary value and does not seem to further decrease. The magnetic components with finite m and/or n disappear as time progresses as shown in Fig. 6, although only the $(m, n) = (-2, 1)$ components are shown. We obtained similar results in Sec. IV A 6 for the other initial perturbation. Therefore, SA seems to recover the original cylindrical symmetric equilibrium. This is of course reasonable since the original equilibrium is linearly stable against ideal MHD modes. In fact, the total energy is almost the same as that of the original equilibrium; it is larger than the original one by $\mathcal{O}(10^{-10})$ for the case of Sec. IV A 5 and $\mathcal{O}(10^{-9})$ for the case of Sec. IV A 6, of which relative magnitudes to the total energy of the original equilibrium are $\mathcal{O}(10^{-9})$ and $\mathcal{O}(10^{-8})$, respectively.

Thus, here we have shown two cases where SA recovers the original equilibrium if it is ideal MHD stable. Another case was performed with $r_0 = 0.8$ in Eqs. (14) and (15), with similar amplitudes as in Fig. 2. The perturbation in this case exists mainly in the region outside the $q = 2$ surface, which is resonant with the family of $(m, n) = (-2, 1)$ harmonics. For this case we obtained qualitatively similar results.

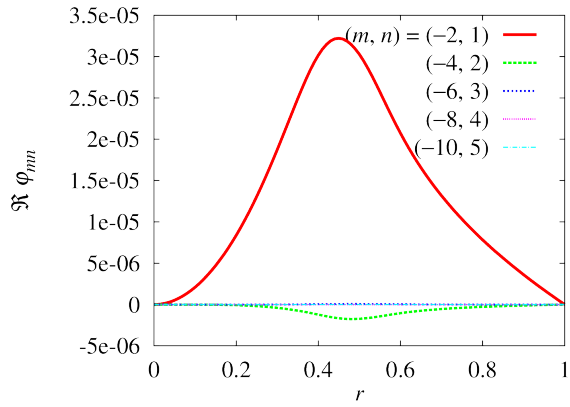
For an unstable equilibrium case, SA finds growth of the dynamically accessible pertur-



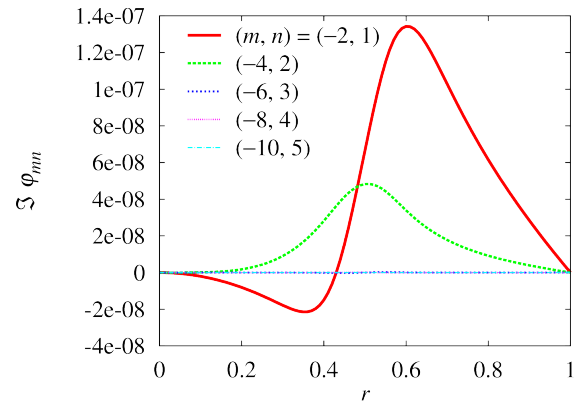
(a) Radial profile of $\Re U_{mn}$.



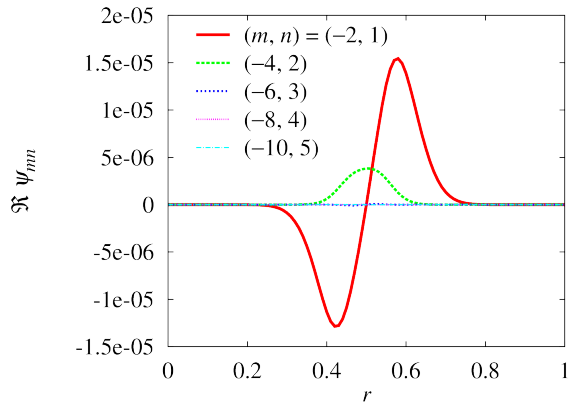
(b) Radial profile of $\Im U_{mn}$.



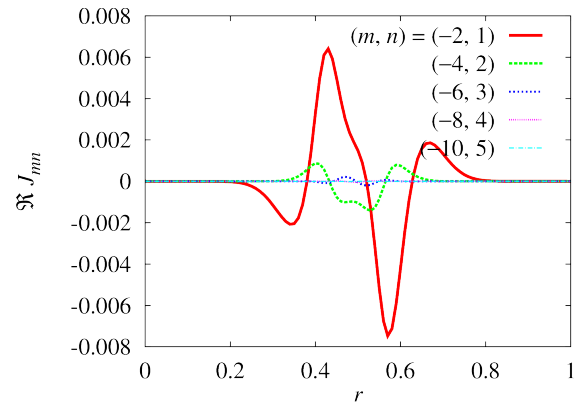
(c) Radial profile of $\Re \varphi_{mn}$.



(d) Radial profile of $\Im \varphi_{mn}$.



(e) Radial profile of $\Re \psi_{mn}$. The imaginary part is zero.



(f) Radial profile of $\Re J_{mn}$. The imaginary part is zero.

FIG. 14: Radial profiles of the perturbed state that is used as an initial condition for SA. The $(m, n) = (-2, 1)$ components are dominant, but they still have small amplitudes.

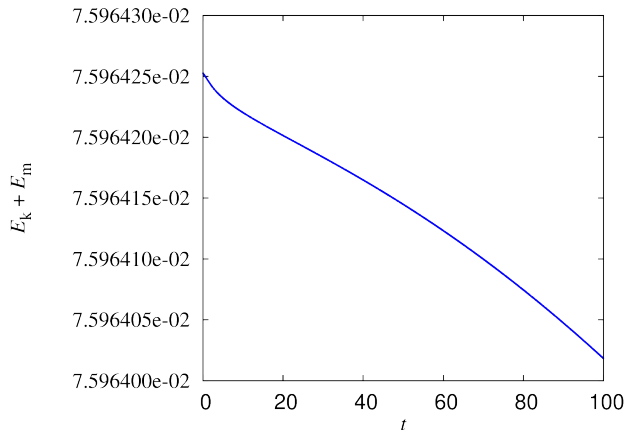
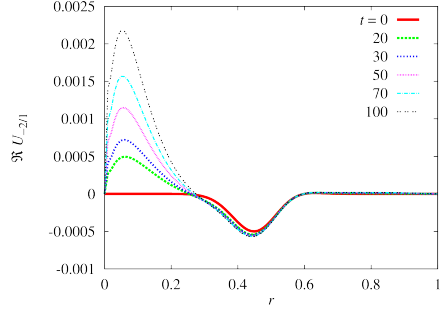


FIG. 15: The total energy decreased in time by SA, although the perturbation amplitudes grew in time as shown in Fig. 16

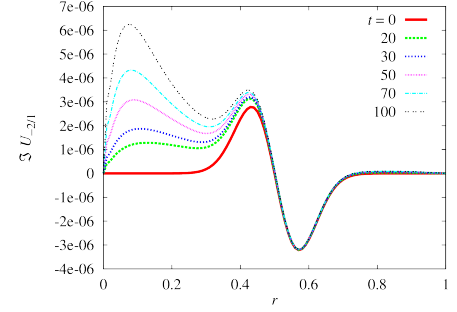
bation in time under decreasing total energy. We expect the SA procedure, in principle, will converge to another equilibrium if there is one on the same Casimir leaf and the perturbation lies within its basin of attraction. In the case tried in this paper, however, the physical situation seems to be tough for numerical study, and only linear stability was examined.

V. CONCLUSIONS

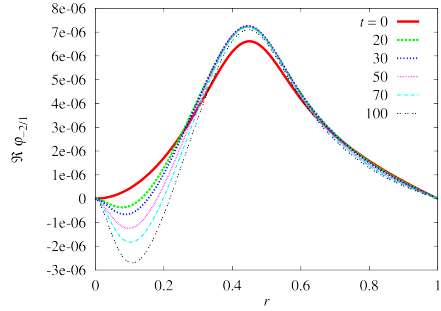
In this paper, simulated annealing (SA) was applied to low-beta reduced magnetohydrodynamics (MHD) in cylindrical geometry. Specifically, SA was used to verify the stability of a cylindrically symmetric equilibrium, which is known to be linearly stable or unstable against ideal MHD modes. To this end, a dynamically accessible perturbation was added to the cylindrically symmetric equilibrium by introducing advection fields for perturbing the equilibrium without leaving the Casimir leaf on which the original symmetric equilibrium exists. The dynamically accessible perturbation increased (decreased) the total energy of the system if the original equilibrium is linearly stable (unstable). Then SA was performed to monotonically decrease the total energy. It was found that the SA reasonably recovers the original, cylindrically symmetric equilibrium when it is stable. On the other hand, the perturbation grew when the original equilibrium is unstable. Since low-beta reduced MHD is a two-field model, it has two advection fields for relaxation. It was found that for practical implementation of SA, it is important to balance the order of magnitude of the two advection fields for SA relaxation to occur on a short time scale. To achieve such efficient



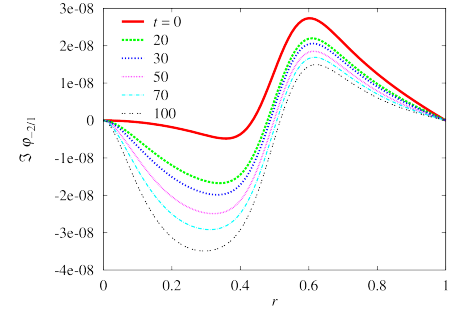
(a) Radial profile of $\Re U_{-2,1}$.



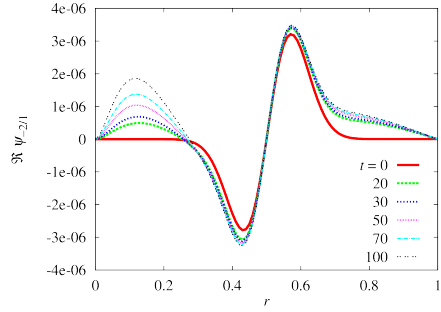
(b) Radial profile of $\Im U_{-2,1}$.



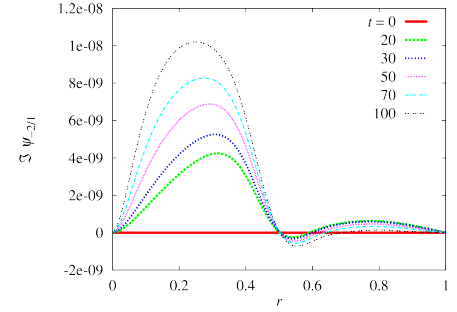
(c) Radial profile of $\Re \varphi_{-2,1}$.



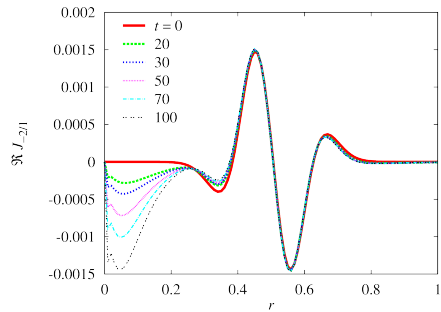
(d) Radial profile of $\Im \varphi_{-2,1}$.



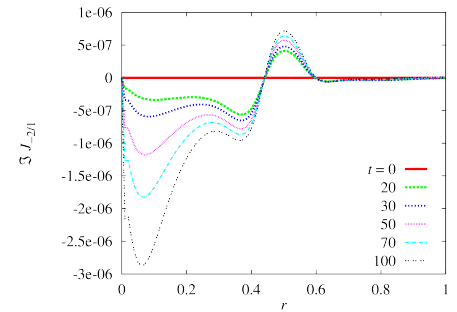
(e) Radial profile of $\Re \psi_{-2,1}$.



(f) Radial profile of $\Im \psi_{-2,1}$.



(g) Radial profile of $\Re J_{-2,1}$.



(h) Radial profile of $\Im J_{-2,1}$.

FIG. 16: Radial profiles of the $(m, n) = (-2, 1)$ components are plotted at several times during the SA evolution. The perturbation amplitudes grew in time.

relaxation, time dependence was introduced in the symmetric kernel of SA, in such a way as to balance the orders of magnitude of the two advection fields, thereby leading to accelerated convergence to the minimum energy state. The acceleration is particularly necessary for a stable equilibrium, since we have to observe that the perturbation actually disappears.

In essence, the SA method provides a general prescription for building from a Hamiltonian system an alternative non-Hamiltonian system with asymptotic stability to an equilibrium state, with the stability provided by an energy function serving as a Lyapunov function. Convergence to the equilibrium requires that the Lyapunov function have a local extremum, which is enough to show stability for the original Hamiltonian system. Systems that are spectrally stable need not have Lyapunov functions (because of negative energy modes, see e.g. Ref. 2) so the SA method here provides a method that singles out systems that are likely to be nonlinearly stable. Given this general framework, there are many avenues for further explorations in the context of fluid and kinetic plasma models.

ACKNOWLEDGMENTS

MF was supported by JSPS KAKENHI Grant Number JP21K03507 while PJM was supported by the U.S. Dept. of Energy Contract # DE-FG05-80ET-53088 and the Humboldt Foundation. We both would like to acknowledge the JIFT program for support of MF to visit IFS in the Spring of 2019 when a portion of this work was carried out.

REFERENCES

- ¹G. R. Flierl, P. J. Morrison, “Hamiltonian-Dirac simulated annealing: Application to the calculation of vortex states,” *Physica D* **240**, 212 (2011) .
- ²P. J. Morrison, “Hamiltonian description of the ideal fluid,” *Rev. Mod. Phys.* **70**, 467 (1998).
- ³M. D. Kruskal and C. R. Oberman, “On the stability of plasma in static equilibrium,” *Phys. Fluids* **1**, 275–280 (1958).
- ⁴V. I. Arnol’d, “Variational principle for three-dimensional steady-state flows of an ideal fluid,” *Prikl. Math. Mech.* **29**, 846–851 (1965), [English transl. *J. Appl. Maths Mech.* **29**, 1002–1008 (1965)].

- ⁵G. K. Vallis, G. F. Carnevale and W. R. Young, “Extremal energy properties and construction of stable solutions of the Euler equations,” *J. Fluid Mech.* **207**, 133–152 (1989).
- ⁶G. F. Carnevale and G. K. Vallis, “Pseudo-advective relaxation to stable states of inviscid two-dimensional fluids,” *J. Fluid Mech.* **213**, 549–571 (1990).
- ⁷T. G. Shepherd, “A general method for finding extremal states of Hamiltonian dynamic systems, with applications to perfect fluids,” *J. Fluid Mech.* **213**, 573 (1990).
- ⁸P. J. Morrison and J. M. Greene, “Non-canonical Hamiltonian Density Formulation of Hydrodynamics and Ideal Magnetohydrodynamics,” *Phys. Rev. Lett.* **45**, 790 (1980).
- ⁹Y. Chikasue and M. Furukawa, “Simulated annealing applied to two-dimensional low-beta reduced magnetohydrodynamics,” *Phys. Plasmas* **22**, 022511 (2015).
- ¹⁰Y. Chikasue and M. Furukawa, “Adjustment of vorticity fields with specified values of Casimir invariants as initial condition for simulated annealing of an incompressible, ideal neutral fluid and its MHD in two dimensions,” *J. Fluid Mech.* **774**, 443 (2015).
- ¹¹H. R. Strauss, “Nonlinear, three-dimensional magnetohydrodynamics of noncircular tokamaks,” *Phys. Fluids* **19**, 134 (1976).
- ¹²M. Furukawa and P. J. Morrison, “Simulated annealing for three-dimensional low-beta reduced mhd equilibria in cylindrical geometry,” *Plasma Phys. Control. Fusion* **59**, 054001 (2017).
- ¹³H. R. Strauss, “Dynamics of high β tokamaks,” *Phys. Fluids* **20**, 1354–1360 (1977).
- ¹⁴M. Furukawa, Takahiro Watanabe, P. J. Morrison, and K. Ichiguchi, “Calculation of large-aspect-ratio tokamak and toroidally-averaged stellarator equilibria of high-beta reduced magnetohydrodynamics via simulated annealing,” *Phys. Plasmas* **25**, 082506 (2018).
- ¹⁵P. J. Morrison, “Structure and structure-preserving algorithms for plasma physics,” *Phys. Plasmas* **24**, 055502 (2017).
- ¹⁶P. J. Morrison, “A Paradigm for Joined Hamiltonian and Dissipative Systems,” *Physica D* **18**, 410 (1986).
- ¹⁷C. Bressan, M. Kraus, P. J. Morrison, and O. Maj, “Relaxation to magnetohydrodynamics equilibria via collision brackets,” *Journal of Physics: Conference Series* **1125**, 012002 (2018).
- ¹⁸V. D. Shafranov, “On magnetohydrodynamical equilibrium configurations,” *Soviet Physics JETP* **6**, 545 (1958).
- ¹⁹R. Lüst and A. Schlüter, *Zeitschrift für Naturforschung* **12A**, 850 (1957).

- ²⁰H. Grad and H. Rubin, in *Proceedings of the Second United Nations International Conference on the Peaceful Uses of Atomic Energy*, Vol. 31 (United Nations, Geneva, 1958).
- ²¹J. A. Nelder and R. Mead, “A Simplex Method for Function Minimization,” *The Computer Journal* **7**, 308–313 (1965).
- ²²John H. Holland, *Adaptation in Natural and Artificial Systems: An Introductory Analysis with Applications to Biology, Control and Artificial Intelligence* (The University of Michigan Press, Ann Arbor, 1975).
- ²³P. J. Morrison and D. Pfirsch, “Free Energy Expressions for Vlasov Equilibria,” *Phys. Rev. A* **40**, 3898–3910 (1989).
- ²⁴P. J. Morrison and D. Pfirsch, “The Free Energy of Maxwell-Vlasov Equilibria,” *Phys. Fluids B* **2**, 1105–1113 (1990).
- ²⁵T. Andreussi, P. J. Morrison, and F. Pegoraro, “Hamiltonian Magnetohydrodynamics: Lagrangian, Eulerian, and Dynamically Accessible Stability - Examples with Translation Symmetry,” *Phys. Plasmas* **23**, 102112 (2016).
- ²⁶P. J. Morrison and R. D. Hazeltine, “Hamiltonian Formulation of Reduced Magnetohydrodynamics,” *Phys. Fluids* **27**, 886–897 (1984).
- ²⁷J. E. Marsden and P. J. Morrison, “Noncanonical Hamiltonian Field Theory and Reduced MHD,” *Contemp. Math.* **28**, 133–150 (1984).